Biophysical Journal
Article

Biophysical Society

# Modulation of DEG/ENaCs by Amphiphiles Suggests Sensitivity to Membrane Alterations

Axel Schmidt,[1] Rick J. Alsop,[2] Rahul Rimal,[1] Pia Lenzig,[1] Sylvia Joussen,[1] Natalie N. Gervasi,[2] Adree Khondker,[2] Stefan Gründer,[1] Maikel C. Rheinstädter,[2] and Dominik Wiemuth[1,*]
[1]Institute of Physiology, RWTH Aachen University, Aachen, Germany and [2]Department of Physics and Astronomy, McMaster University, Hamilton, Ontario, Canada

ABSTRACT The bile acid-sensitive ion channel is activated by amphiphilic substances such as bile acids or artificial detergents via membrane alterations; however, the mechanism of membrane sensitivity of the bile acid-sensitive ion channel is not known. It has also not been systematically investigated whether other members of the degenerin/epithelial $Na^+$ channel (DEG/ENaC) gene family are affected by amphiphilic compounds. Here, we show that DEG/ENaCs ASIC1a, ASIC3, ENaC, and the purinergic receptor P2X2 are modulated by a large number of different, structurally unrelated amphiphilic substances, namely the detergents N-lauroylsarcosine, Triton X-100, and $\beta$-octylglucoside; the fenamate flufenamic acid; the antipsychotic drug chlorpromazine; the natural phenol resveratrol; the chili pepper compound capsaicin; the loop diuretic furosemide; and the antiarrythmic agent verapamil. We determined the modification of membrane properties using large-angle x-ray diffraction experiments on model lipid bilayers, revealing that the amphiphilic compounds are positioned in a characteristic fashion either in the lipid tail group region or in the lipid head group region, demonstrating that they perturbed the membrane structure. Collectively, our results show that DEG/ENaCs and structurally related P2X receptors are modulated by diverse amphiphilic molecules. Furthermore, they suggest alterations of membrane properties by amphiphilic compounds as a mechanism contributing to modulation.

## INTRODUCTION

Members of the degenerin/epithelial $Na^+$ channel (DEG/ENaC) family of ion channels contribute to diverse physiological functions ranging from transepithelial transport to sensation of various external stimuli and synaptic transmission (1,2). DEG/ENaCs are characterized by a conserved topology of subunits and a trimeric structure (2,3). Each subunit is composed of a large extracellular domain (ECD), which connects two transmembrane domains (TMDs). The N- and C-termini extend into the cytosol (3).

In vertebrates, the DEG/ENaC family comprises three subgroups (4): the acid-sensing ion channels (ASICs), the epithelial $Na^+$ channel (ENaC), and the bile acid-sensitive ion channel (BASIC) (4). ASICs are ligand-gated neuronal channels with protons as ligands. They are activated by a sudden increase in the extracellular proton concentration (5). In the central nervous system, ASICs are involved in synaptic transmission and have been associated with different neuronal disorders (6–8). In the peripheral nervous system, ASICs, in particular ASIC3, are involved in nociception and mechanosensation (9–14). ENaC is responsible for the absorption of $Na^+$ in a variety of different epithelia (15). BASIC forms the third subfamily. It is expressed in the brain, the liver, and the intestinal tract and is activated by bile acids; its function is not clear yet (4). Within the DEG/ENaC family, ENaC and BASIC have been shown to be sensitive to changes in membrane properties induced by amphiphilic substances (16,17), but a systematic analysis of the influence of amphiphiles on other DEG/ENaCs is lacking so far.

The ionotropic purinergic P2X receptors are not related to DEG/ENaCs; however, they do share some structural features with them, e.g., a trimeric organization, two TMDs per subunit, and large ECDs (18). P2X receptors are expressed in a large variety of tissues and cells, and their physiological function is equally diverse (19). Some P2X receptors are modulated by specific membrane lipids and cholesterol (20–23), but a dependence of P2X receptor activity on the biophysical properties of the plasma membrane has, to our knowledge, not been described yet.

Various ion channels have been shown to be modulated by membrane alterations induced by amphiphilic molecules;

*Submitted May 2, 2017, and accepted for publication January 26, 2018.*
*Correspondence: dwiemuth@ukaachen.de
Editor: Michael Pusch.
https://doi.org/10.1016/j.bpj.2018.01.028

e.g., Triton X-100 and β-octylglucoside shift the voltage-dependence of $Na^+$ channel inactivation (24), and resveratrol and capsaicin inhibit Kv2.1 and the mechanosensitive ion channel MscL (25). Depending on the preferred site of plasma membrane insertion, amphiphilic substances may affect bilayer properties differently (26,27). Two-dimensional x-ray diffraction of artificial lipid bilayers enables determination of their molecular structure and orientation and identification of the localization of amphiphilic molecules within the bilayer (28–32).

In this study, we systematically analyzed the effect of a variety of structurally diverse amphiphilic molecules on the activity of ASIC1a, ASIC3, ENaC, gramicidin A, and the purinergic ionotropic receptor P2X2. We show that all these channels are affected in varying degrees by the molecules tested, suggesting that amphiphile sensitivity is a common feature within the DEG/ENaC family. Moreover, we tested the effect of the amphiphilic molecules on membrane properties using x-ray diffraction and compared it with their functional effect. Finally, we analyzed the conformational changes in established structures of cASIC1 and zP2X4 between conducting and nonconducting states. Our results are in line with the idea that membrane properties play an important role for channel function. Therefore, nonspecific membrane-mediated side effects should be considered carefully when evaluating specific molecules targeting members of the DEG/ENaC family.

## MATERIALS AND METHODS

### Molecular biology

The SP6 mMessage mMachine kit (Ambion, Austin, TX) was used to amplify capped cRNA coding for rat ASIC1a (rASIC1a); rat ASIC3 (rASIC3); α-, β-, and γ-rat ENaC (rENaC); and rat P2X2 (rP2X2) from linearized plasmids.

### Two-electrode voltage-clamp in *Xenopus laevis* oocytes

Animal care and experimental protocols were approved by the Landesamt für Natur, Umwelt und Verbraucherschutz of North Rhine-Westphalia and were performed in accordance with their guidelines. Oocytes were surgically removed as described previously (33). Anesthetized frogs were sacrificed by decapitation after the final oocyte collection. The following amounts of cRNA were injected into stage V or VI oocytes of *X. laevis*: rASIC1a, 0.016 ng; rASIC3, 2–8 ng; αβγrENaC (1:1:1 ratio), 0.16 ng; and rP2X2, 0.04 ng. Oocytes were kept in Oocyte Ringer-2 medium (in mM, 82.5 NaCl, 2.5 KCl, 1 $Na_2HPO_4$, 10 HEPES, 1.0 $MgCl_2$, 1 $CaCl_2$, and 0.5 mg/mL polyvinylpyrrolidone), with the exception of ENaC-expressing oocytes, which were kept in low-$Na^+$ Oocyte Ringer-2 medium (in mM, 5 NaCl, 77.5 *N*-methyl-D-glucamine, 2.5 KCl, 1 $Na_2HPO_4$, 10 HEPES, 1.0 $MgCl_2$, 1 $CaCl_2$, and 0.5 mg/mL polyvinylpyrrolidone) at 19°C. Whole cell currents were recorded 24–72 h postinjection at room temperature (20–25°C) with a TurboTec 03X amplifier (npi electronic, Tamm, Germany). Oocytes were superfused using a fast, pump-driven automatic solution exchange system (npi electronic) (34,35). Data acquisition and solution exchange were performed using CellWorks 5.1.1 (npi electronic). Data were acquired at 200 Hz and filtered at 20 Hz. Holding potential was −70 mV. Standard bath solution for two-electrode voltage-clamp measurements contained (in mM) 140 NaCl, 1.8 $CaCl_2$, 1 $MgCl_2$, and 10 HEPES (pH 7.4) or 10 2-(N-morpholino)ethanesulfonic acid (pH 6.5). rP2X2-expressing oocytes were injected with 50 nL chelating buffer (in mM, 20 EGTA, 10 HEPES, pH 7.4) 15–120 min before recording.

*N*-lauroylsarcosine (NL), Triton X-100 (TX), chlorpromazine (CPZ), gramicidin A (gA), verapamil (VP), resveratrol (RV), furosemide (FS), capsaicin (CAP), and flufenamic acid (FFA) were purchased from Sigma-Aldrich (Munich, Germany); β-octylglucoside (βOG) was purchased from Cayman Chemicals (Ann Arbor, MI).

Stock solutions of FFA (100 mM), RV (20 mM), CAP (100 mM), and gA (20 mM) were prepared in dimethyl sulfoxide (DMSO). All other compounds were dissolved in standard bath solution. gA measurements were performed by applying freshly prepared 40 μM gA in standard bath solution containing 0.2% DMSO. For the electrophysiological experiments, high micromolar but nonsolubilizing concentrations of the amphphilic substances were chosen.

### Preparation of synthetic membrane samples

Highly oriented, multilamellar membranes were prepared on polished 1 × 1 $cm^2$ silicon wafers. The wafers were first pretreated by sonication in dichloromethane at 310 K for 25 min to remove all organic contamination and create a hydrophobic substrate. After removal from the dichloromethane postsonication, each wafer was thoroughly rinsed three times by alternating with ∼50 mL of ultrapure water and methanol.

1,2-dimysteroyl-sn-glycero-3-phosphocholine (DMPC) was obtained from Avanti Polar Lipids (Alabaster, AL) and dissolved in 1:1 mixtures of chloroform and tri-fluoro-ethanol. NL, TX, CPZ, FFA, VP, RV, FS, CAP (Sigma), and βOG (Cayman Chemicals) were also dissolved in mixtures of 1:1 tri-fluoro-ethanol:chloroform. The DMPC and substance solutions were then mixed in the appropriate ratios (0, 3, and 10 mol% substance in DMPC) to achieve the desired membrane compositions for the experiment.

A tilting incubator was heated to 313 K, and the lipid solutions were placed inside to equilibrate. 80 μL of lipid solution was deposited on each wafer, and the solvent was then allowed to slowly evaporate for ∼10 min while being gently rocked, such that the lipid solution spread evenly on the wafers. After drying, the samples were placed in vacuum at 313 K for 12 h to remove all traces of solvent. Samples were incubated in a sealed container containing an open vial of pure water and allowed to equilibrate to 293 K. The temperature was then slowly increased to 303 K over a period of 24 h. This procedure results in highly oriented, multilamellar membrane stacks and a uniform coverage of the silicon substrates. About 3000 highly-oriented stacked membranes with a total thickness of ∼10 μm are produced using this protocol. The high sample quality and high degree of order is a prerequisite to determine the in-plane and out-of-plane structure of the membrane complexes separately but simultaneously.

Out-of-plane and in-plane x-ray scattering data were obtained using the Biological Large Angle Diffraction Experiment in the Laboratory for Membrane and Protein Dynamics at McMaster University. The Biological Large Angle Diffraction Experiment uses a 9 kW (45 kV, 200 mA) CuK-α Rigaku SmartLab (Rigaku, Tokyo, Japan) rotating anode at a wavelength of 1.5418 Å. Both source and detector are mounted on moveable arms, such that the membranes stay horizontal during measurements. When focusing, multilayer optics provide a high-intensity parallel beam with monochromatic x-ray intensities up to $10^{10}$ counts/(s · $mm^2$). This beam geometry provides optimal illumination of the membrane samples to maximize the scattered signal. By using highly oriented stacks, the in-plane ($q_{||}$) and out-of-plane ($q_z$) structure of the membranes could be determined independently. A sketch of the scattering geometry is depicted in Fig. 1 *A*. The experiment produces two-dimensional intensity maps covering length scales from ∼2 to 200 Å (Fig. 1 *B*). The two-dimensional maps are, for instance, used to calculate the lamellar spacing, $d_z$, and the area-per-lipid, $A_L$. The location

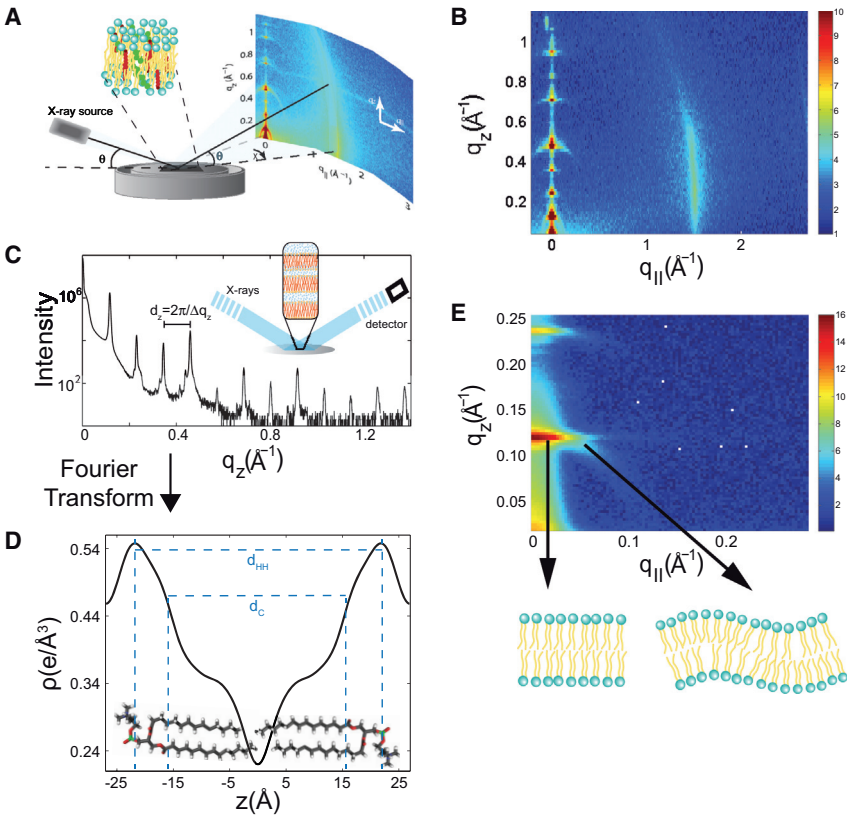


FIGURE 1 X-ray preparation and analysis of highly oriented DMPC membrane samples. (*A*) Two-dimensional x-ray diffraction is used to obtain large maps of reciprocal space of the samples. (*B*) Shown is the reciprocal space map (RSM) for pure DMPC. The map measures $0 < q_z < 1.1$ Å$^{-1}$ and $-0.3$ Å$^{-1} < q_{||} < 3.0$ Å$^{-1}$, covering length scales of 2 Å up to 200 Å. (*C*) Shown is the out-of-plane ($q_z$) reflectivity for a DMPC sample. The bilayer spacing, $d_z$, is determined from the spacing between Bragg peaks. (*D*) An electron density profile for DMPC membranes is shown. The absolute maximum in the curve is associated with the electron-rich phosphate head group of the DMPC molecule. Head-head spacing ($d_{HH}$) and hydrophobic chain length ($d_C$) can be determined from the profile. (*E*) A RSM at low $q$ for DMPC is shown.

of the molecules in the bilayer was extracted from out-of-plane (reflectivity) scans (Fig. 1 *C*), which were Fourier-transformed to calculate the electron density, $\rho$, perpendicular to the membranes (Fig. 1 *D*). In addition, higher resolution two-dimensional maps were acquired (Fig. 1 *E*) to measure bilayer orientation, $H$ (28–32,36,37), and bending.

## Out-of-plane structure and electron densities

An example out-of-plane ($q_z$) scan is displayed in Fig. 1 *C*. Electron density profiles are reconstructed from the out-of-plane scattering, as detailed in (28,30–32,36). An example density profile is shown in Fig. 1 *D*. The absolute maximum in the profile corresponds to the electron-rich lipid head group, with $z = 0$ corresponding to the center of the bilayer between the acyl chains of opposing leaflets. The lipid head-head distance, $d_{HH}$, is found by measuring the position of the head group maximum. The length of the chain region, $2d_C$, is calculated by $2d_C = d_{HH} - 2d_{HI}$, with $d_{HI} = 5$ Å. $d_{HI}$ represents the distance from the head group peak to the interface between the head group and tail group. We determined $d_C = 16 \pm 1$ Å for a pure DMPC.

## Estimation of partitioning coefficients and of membrane concentrations of amphiphilic substances

To estimate the partitioning coefficients of each substance, the difference in electron density between a pure DMPC bilayer and a bilayer with the substance embedded at 3 mol% of the initial lipid-membrane composition was determined and converted into a total number of electrons. By dividing this number by the theoretical number of electrons from the molar mass and concentration of the substance, the total partitioning of the substance into the membrane (i.e., [membrane]/[solution]) was calculated. The corresponding values are given in Table 1. The concentrations of the substances in the plasma membrane of oocytes were estimated as follows: oocytes have a diameter of ~1 mm. The oocyte plasma membrane is highly folded into macro and microvilli, thereby increasing the apparent surface area by a factor of 4. The actual surface area was reported to be between 18 (38) and 20 mm$^2$ (39). An average-area-per-lipid-molecule in fluid lipid membranes was reported to be ~60 Å$^2$ (40). By assuming a protein content of 20%, the amount of lipids (in moles) was then calculated by dividing the membrane area by the area per lipid molecule to $0.80 \times 2 \times 10^{-5}/(6 \times 10^{-19} \times 6 \times 10^{23}) = 4.44 \times 10^{-11}$ moles (with $6 \times 10^{23}$ as Avogadro's number). We estimated that the membrane was in direct contact with a volume of solution corresponding to a sphere with a diameter of 2 mm. The number of substance molecules interacting with the membranes was then calculated to the following: $4/3\pi(1 \times 10^{-3})^3$[subst.]. By including the partitioning coefficient determined by x-ray analysis, the amount of substances in the oocyte membranes was estimated. A complete list of concentrations for all substances is listed in Table 1.

## Modeling and structural analysis of ASIC1 and P2X4

Structures of cASIC1 in the open and the desensitized state were modeled based on the Protein Data Bank (PDB) structures 4NTW and 4NYK, respectively, using Modeler 9.16 (41). Likewise, structures of zP2X4 in the closed and the open state were modeled based on the PDB structures 4DW0 and 4DW1, respectively. For easier comparison, sequences were truncated to account for different lengths of the crystallized proteins (cASIC1: 45–453 and P2X4: 36–359). Cross-sectional diameter profiles were generated as follows: first, the central channel axis was determined by utilizing the composition of three subunits and the almost-perfect threefold rotational symmetry of the structural models. In detail, centroids of triangles defined by the sets of three corresponding atoms between channel subunits were determined. These centroids were fitted by a regression line, which was

**TABLE 1 Partitioning Coefficients and Concentrations of Amphiphilic Substances in X-Ray Membrane Analysis and Electrophysiological Ion Channel Analysis**

| | X-Ray Membrane Analysis | | Electrophysiological Ion Channel Analysis | |
|---|---|---|---|---|
| Substance | Partitioning Coefficients (Membrane/Water) | Concentration in Membrane (mol%) | Concentration in Bath Solution (mM) | Concentration in Membrane (mol%) |
| CPZ | 0.330 | 0.991 | 0.25 | 0.778 |
| NL | 0.355 | 1.065 | 0.5 | 1.673 |
| TX | 0.161 | 0.482 | 0.1 | 0.151 |
| FFA | 0.130 | 0.390 | 1 | 1.224 |
| $\beta$OG | 0.144 | 0.432 | 5 | 6.778 |
| RV | 0.434 | 1.303 | 0.1 | 0.409 |
| CAP | 0.328 | 0.984 | 0.25 | 0.773 |
| FS | 0.036 | 0.109 | 1 | 0.343 |
| VP | 0.225 | 0.674 | 1 | 2.117 |

Note that concentrations of substances in x-ray membrane analysis were estimated from electron density data of DMPC membranes with an initial lipid-substance composition of 3 mol%.

considered as the central channel axis. Next, the distance of each atom to the central channel axis was measured and plotted against the atom's position relative to the central channel axis. To achieve this, planes were derived from the coordinates of three corresponding atoms, and their intersection points with the central channel axis were calculated. The distance between each atom and its corresponding intersection point was calculated. For the three corresponding atoms, these distances were averaged to compensate for minor fluctuations introduced by structural modeling. Finally, these averaged distances were plotted against the position of the intersection points on the central channel axis. Minimal, maximal, and average distances to the central channel axis were calculated for layers of 1.5 Å and depicted as lines in Fig. 10.

The position of the lipid bilayer relative to the protein was estimated by the distribution of hydrophobic residues within the TMDs and by examination of lipid-bilayer-embedded structures from MemProtMD (42). The calculation was checked by graphical representation and visual inspection of the results of all intermediate steps.

## Data analysis

Data were collected and pooled from at least two preparations of oocytes isolated from different animals, if not stated otherwise. Electrophysiological recordings were analyzed with IgorPro 5.0.3 (Wavemetrics, Lake Oswego, OR). Desensitization time constants ($\tau$) were determined by single exponential fits of current decay for rASIC1a and rASIC3. Statistical analysis was performed in R 3.4.2 (R Core Team, Vienna, Austria). Data are reported as mean ± SE, and statistical significance was calculated using a Student's unpaired $t$-test followed by Bonferroni's correction, in which $p$-values were multiplied by the number of comparisons to yield a corrected $p$-value. Corrected values of $p < 0.05$ were considered statistically significant. Current traces and bar graphs were plotted with IgorPro.

# RESULTS

## Modulation of rASIC1a by structurally divergent amphiphilic molecules

To determine whether rASIC1a activity can be modulated by amphiphilic substances, we chose nine molecules that shared no structural similarities except their amphiphilic nature: NL, an anionic tenside containing a hydrophobic 12-carbon chain and a hydrophilic carboxylate; $\beta$OG, a nonionic surfactant based on octanol and glucoside; FFA, an anthranilic acid derivative; TX, a nonionic surfactant containing a polyethylene chain and an aromatic hydrocarbon group; CPZ, a phenothiazine derivative, a heterotricyclic group containing a dimethylpropane amine chain; RV, a naturally occurring stilbenoid; CAP, the active alkaloid compound of chili peppers; VP, a phenylalkylamine derivative; and FS, a benzoic-sulfonamide-furan (Fig. 2).

rASIC1a expressed in *Xenopus* oocytes was activated by repetitive application of a pH 6.5 solution. Channel modulation by amphiphilic substances was tested by applying either 500 $\mu$M NL, 5 mM $\beta$OG, 1 mM FFA, 100 $\mu$M TX, 250 $\mu$M CPZ, 100 $\mu$M RV, 250 $\mu$M CAP, 1 mM VP, or 1 mM FS (Fig. 3 *A*) for 10 s before and during the pH 6.5 activation

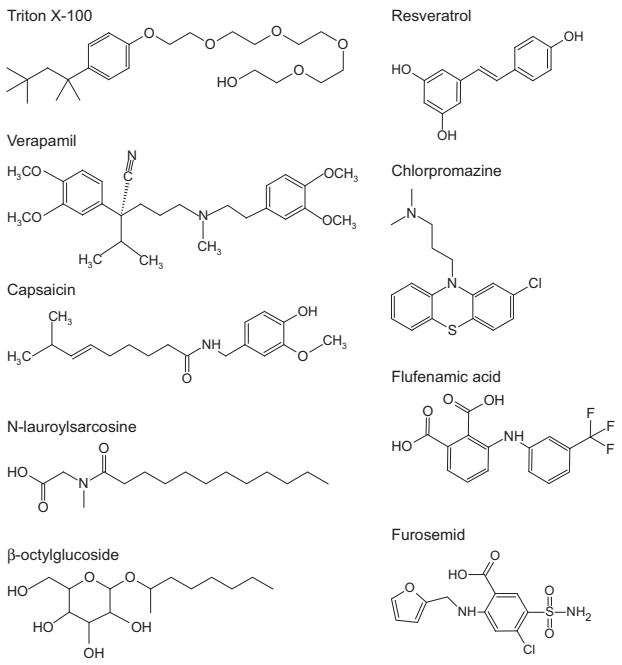


FIGURE 2 Structures of the amphiphilic molecules used in this study. Structures were drawn using CambridgeSoft ChemDraw Ultra (CambridgeSoft, Waltham, MA) based on structures available from PubChem (http://pubchem.ncbi.nlm.nih.gov/).

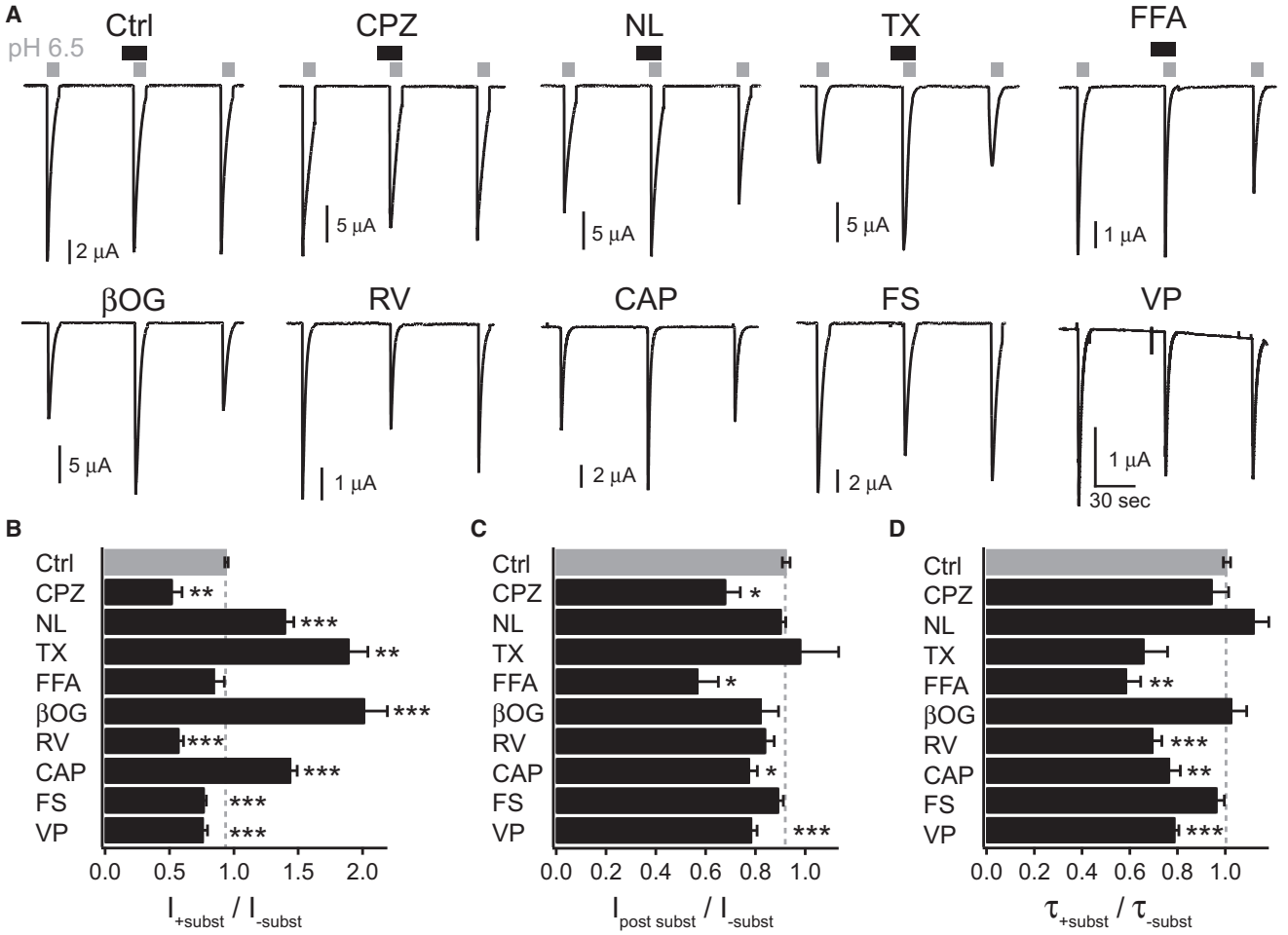


FIGURE 3 rASIC1a modulation by amphiphilic substances. (*A*) Representative current traces of oocytes expressing rASIC1a repeatedly activated by proton application are shown (pH 6.5, *gray bars*). Bath solution without amphiphiles (Ctrl) or with 250 $\mu$M chlorpromazine (CPZ), 500 $\mu$M *N*-lauroylsarcosine (NL), 100 $\mu$M Triton X-100 (TX), 1 mM flufenamic acid (FFA), 5 mM $\beta$-octylglucoside ($\beta$OG), 100 $\mu$M resveratrol (RV), 250 $\mu$M capsaicin (CAP), 1 mM furosemid (FS), or 1 mM verapamil (VP) was present during the time indicated by the black bar. (*B*) Quantitative analysis of peak currents in the presence of the substances, normalized to the previous activation in the absence of the substances. The mean amplitude of the first activation ranged from $-20 \pm 1.9$ $\mu$A to $-4.8 \pm 1$ $\mu$A (control $-12.2 \pm 1.5$ $\mu$A, n = 9–45). (*C*) Quantification of mean currents of the last peak were normalized to the first peak current. (*D*) The mean desensitization constants $\tau_{des}$ in the presence of the substances were normalized to the previous activation in the absence of the substances. The mean $\tau_{des}$ of the first activation ranged from $3.9 \pm 0.4$ to $2.5 \pm 0.3$ s (control $3.3 \pm 0.2$ s, n = 5–43). Bars represent the mean, and the error bars represent the mean $\pm$ SE (*$p < 0.05$, **$p < 0.01$, ***$p < 0.001$).

(pre- and coapplication). None of the substances activated rASIC1a when applied alone, but all substances induced an altered response to pH 6.5 application (Fig. 3 *A*). NL, TX, $\beta$OG, and CAP increased the peak current amplitude, whereas CPZ, RV, FS, and VP decreased it. $\beta$OG and TX had the strongest effects ($I_{+\beta OG}/I_{-\beta OG} = 2.02 \pm 0.17$, n = 13; $I_{+TX}/I_{-TX} = 1.9 \pm 0.14$, n = 9), and NL and CAP affected the pH 6.5 response to a lesser extent ($I_{+NL}/I_{-NL} = 1.4 \pm 0.06$, n = 17; $I_{+CAP}/I_{-CAP} = 1.2 \pm 0.07$, n = 16). CPZ decreased the rASIC1a response to pH 6.5 application most strongly ($I_{+CPZ}/I_{-CPZ} = 0.52 \pm 0.07$, n = 14) followed by RV, VP, and FS, which decreased the pH 6.5 response to a lesser extent ($I_{+RV}/I_{-RV} = 0.57 \pm 0.03$, n = 20; $I_{+VP}/I_{-VP} = 0.76 \pm 0.03$, n = 16; $I_{+FS}/I_{-FS} = 0.77 \pm 0.02$, n = 15). FFA had no significant effect on pH-6.5-induced rASIC1a current amplitudes (Fig. 3, *A* and *B*). Interestingly, some substances (CPZ, FFA, CAP, and VP) significantly reduced rASIC1a peak current amplitudes even after washout (Fig. 3 *C*). This might be explained by the continued presence of the substances in the membrane. Analysis of the desensitization time constant $\tau_{des}$ of rASIC1a revealed that FFA, RV, CAP, and VP significantly accelerated desensitization (Fig. 3, *A* and *D*), whereas the other substances did not significantly affect rASIC1a desensitization.

Taken together, these data show that rASIC1a is indeed sensitive to a variety of amphiphilic compounds.

Next, we tested whether the observed effects of the amphiphilic substances were also detectable after their removal from the bath solution. To address this, we applied

the amphiphilic substances only before and not during the pH 6.5 activation (preapplication) (Fig. 4 *A*). The effects of preapplication of the amphiphilic substances on current amplitude and desensitization of rASIC1a were partly similar to those of pre- and coapplication. NL, TX, and $\beta$OG significantly increased, whereas CPZ and RV significantly decreased peak current amplitude. However, except for CPZ, the effects were significantly weaker when compared to those of pre- and coapplication (Fig. 3 *B*, $p < 0.05$). Desensitization of rASIC1a was accelerated only by TX and VP (Fig. 4, *A–C*), but the effect of VP was significantly weaker when compared to that of pre- and coapplication. In contrast to pre- and coapplication of FFA, RV, and CAP, their pre-applications were significantly ($p < 0.05$) different, as they did not affect the desensitization time constant $\tau_{des}$. Taken together, these data show that some of the substances continue to affect rASIC1a after washout, suggesting that the substances may have accumulated in the membrane.

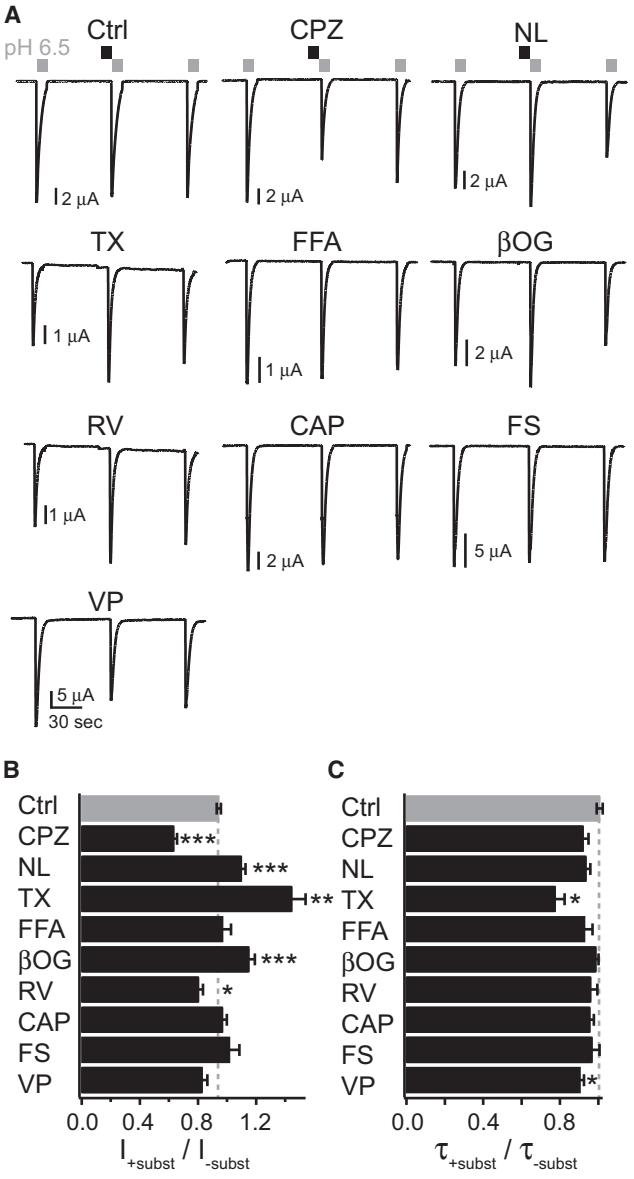


FIGURE 4 rASIC1a modulation by preapplication of amphiphilic substances. (*A*) Representative current traces of oocytes expressing rASIC1a repeatedly activated by proton application are shown (pH 6.5, *gray bar*). Bath solution (Ctrl), 250 $\mu$M CPZ, 500 $\mu$M NL, 100 $\mu$M TX, 1 mM FFA, 5 mM $\beta$OG, 100 $\mu$M RV, 250 $\mu$M CAP, 1 mM FS, or 1 mM VP was present during the time indicated by the black bar. (*B*) Quantitative analysis of the peak currents when substances were preapplied, normalized to the previous activation in absence of the substances. The mean amplitude of the first activation ranged from $-16.1 \pm 3.1$ $\mu$A to $-3.5 \pm 0.3$ $\mu$A (control $-12.2 \pm 1.5$ $\mu$A, n = 7–45). (*C*) Quantitative analysis of the mean desensitization constants $\tau_{des}$ when substances were preapplied, normalized to the $\tau_{des}$ of the previous activation in the absence of the substances. The mean $\tau_{des}$ of the first activation ranged from $3.4 \pm 0.2$ to $2.4 \pm 0.2$ s (control $-3.3 \pm 0.2$ s, n = 6–43). Bars represent the mean, and the error bars represent the mean $\pm$ SE (*$p < 0.05$, **$p < 0.01$, ***$p < 0.001$).

## Sensitivity of other DEG/ENaCs to amphiphilic molecules

To test whether other DEG/ENaCs are also sensitive to amphiphilic substances, we extended our analysis to rASIC3 and ENaC. rASIC3 was activated using the same protocol as that of rASIC1a: a pH activation was followed by an application of the amphiphilic substances NL, $\beta$OG, FFA, TX, CPZ, RT, CAP, VP, or FS 10 s before and during the pH 6.5 activation. The pH-induced current of rASIC3 had a typical kinetic pattern: a fast-transient response was followed by a smaller sustained current in the continuous presence of protons (Fig. 5 *A*).

NL had the strongest potentiating effect on rASIC3 peak current amplitudes ($I_{+NL}/I_{-NL} = 2.83 \pm 0.28$, n = 21). TX and CAP increased peak current amplitude similarly but not as strongly as NL ($I_{+TX}/I_{-TX}$: $2.12 \pm 0.25$, n = 14; $I_{+CAP}/I_{-CAP}$: $2.21 \pm 0.15$, n = 12). VP, CPZ, and RV strongly decreased peak current amplitude ($I_{+VP}/I_{-VP}$: $0.23 \pm 0.02$, n = 16; $I_{+CPZ}/I_{-CPZ}$: $0.58 \pm 0.05$, n = 23; $I_{+RV}/I_{-RV}$: $0.58 \pm 0.02$, n = 21), and FS slightly decreased ASIC3 current amplitude ($I_{+FS}/I_{-FS}$: $0.83 \pm 0.03$, n = 15). $\beta$OG and FFA had no significant effect on rASIC3 current amplitude. (Fig. 5, *A* and *B*). The sustained current of rASIC3 was affected differently by the amphiphilic substances; although it was mildly decreased by CAP ($I_{sustained+CAP}/I_{+CAP}$: $0.0026 \pm 0.0007$, n = 11), it was strongly increased by CPZ and NL ($I_{sustained+CPZ}/I_{-CPZ}$: $0.11 \pm 0.02$, n = 21; $I_{+NL}/I_{-NL}$: $0.02 \pm 0.004$, n = 14). The other substances did not affect the sustained ASIC3 currents significantly (Fig. 5, *A* and *C*). Desensitization of rASIC3 was decelerated by VP, NL, CPZ, TX, $\beta$OG, and CAP. VP and NL had the strongest effect ($\tau_{+VP}/\tau_{-VP}$: $2.28 \pm 0.31$, n = 13; $\tau_{+NL}/\tau_{-NL}$: $1.84 \pm 0.09$, n = 20), followed by TX, $\beta$OG, CPZ, and CAP ($\tau_{+TX}/\tau_{-TX}$: $1.57 \pm 0.12$, n = 14; $\tau_{+\beta OG}/\tau_{-\beta OG}$: $1.57 \pm 0,13$, n = 10; $\tau_{+CPZ}/\tau_{-CPZ}$: $1.3 \pm 0.1$, n = 21; $\tau_{+CAP}/\tau_{-CAP}$: $1.32 \pm 0.07$, n = 8) (Fig. 5, *A* and *D*). In summary, these data suggest that rASIC3 is also sensitive to amphiphilic

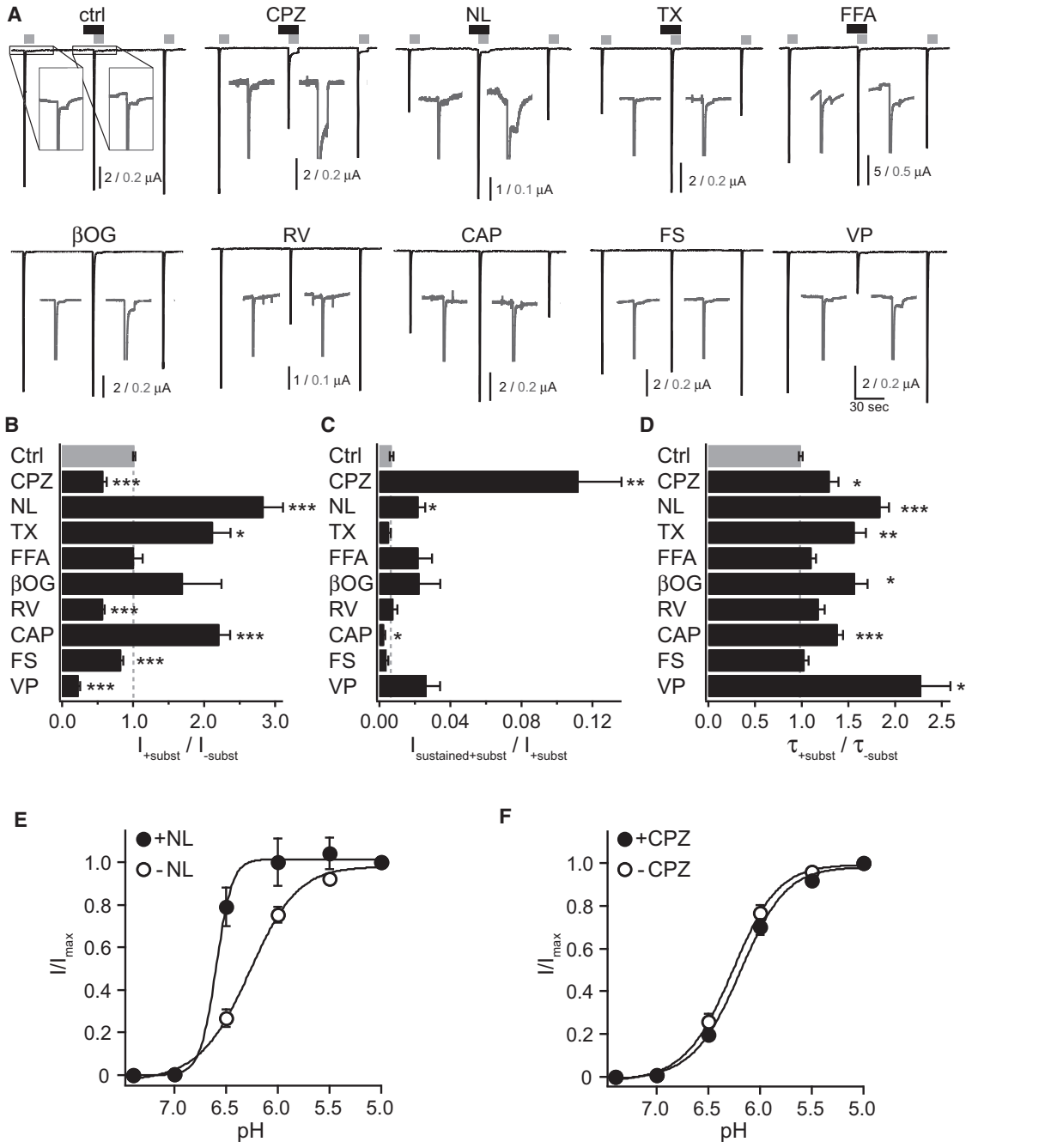


FIGURE 5 rASIC3 is modulated by amphiphilic compounds. (*A*) Representative current traces of rASIC3-expressing oocytes are shown with insets highlighting sustained currents. rASIC3 was repetitively activated by proton application (pH 6.5, *gray bar*). No substance (Ctrl), 250 $\mu$M CPZ, 500 $\mu$M NL, 100 $\mu$M TX, 1 mM FFA, 5 mM $\beta$OG, 100 $\mu$M RV, 250 $\mu$M CAP, 1 mM FS, or 1 mM VP was present in the bath solutions, as indicated by the black bar. (*B*) Quantitative analysis of the peak current amplitudes in the presence of the substances, were normalized to the current amplitude of the previous activation in their absence. For experimental conditions shown, the mean amplitude of the first activation ranged from $-11 \pm 2.1$ to $-4.7 \pm 1$ $\mu$A (control $-10.4 \pm 1.5$ $\mu$A, n = 12–52). (*C*) Quantitative analysis of the sustained current amplitudes, were normalized to the corresponding peak currents in the presence of substances. The mean amplitude of the first activation ranged from $0.08 \pm 0.06$ to $-0.01 \pm 0.003$ $\mu$A, (control $-0.08 \pm 0.02$ $\mu$A, n = 8–35). (*D*) Quantitative analysis of the desensitization constants $\tau_{des}$ in the presence of the substances, normalized to $\tau_{des}$ of the previous activation in the absence of the substances. The mean $\tau_{des}$ of the first activation ranged from $0.4 \pm 0.03$ to $0.3 \pm 0.01$ s (control $0.36 \pm 0.02$ s, n = 10–50). Bars represent the mean, and error bars represent the mean $\pm$ SE (n = 5–52, $*p < 0.05$, $**p < 0.01$, $***p < 0.001$). (*E*) $H^+$ concentration-response curves for rASIC3 in the absence (*open circle*) and presence (*closed circles*) of 500 $\mu$M NL. (*F*) $H^+$ concentration-response curves for rASIC3 in the absence (*open circle*) and presence (*closed circles*) of 250 $\mu$M CPZ. Currents were normalized to the maximal activation at pH 5. Lines represent fits to the Hill equation. Error bars represent the mean $\pm$ SE (n = 7).

compounds. Peak and transient currents as well as desensitization were affected differently.

We hypothesized that amphiphilic substances might influence DEG/ENaCs by favoring certain conformations, thereby shifting the equilibrium between conducting and nonconducting conformations. To test this, we determined the apparent proton affinity of rASIC3 in the presence and absence of the two amphiphilic substances NL and CPZ. NL shifted the apparent affinity from $pH_{50}$ from pH 6.28 ± 0.04 to pH 6.6 ± 0.08 ($p < 0.01$, n = 7), whereas CPZ shifted the apparent proton affinity from $pH_{50}$ from 6.28 ± 0.02 to 6.2 ± 0.03 ($p < 0.05$, n = 7) (Fig. 5, *E* and *F*). These shifts in proton affinities are in line with our hypothesis that the equilibrium of rASIC3 is changed by amphiphilic substances.

To test the sensitivity of ENaC to amphiphilic substances, amiloride-sensitive ENaC currents were recorded in the absence and the presence of the substances. TX, CAP, FS, and VP did not affect ENaC activity, and RV increased amiloride-sensitive ENaC currents ($I_{sub}/I_{ami}$: RV: 1.35 ± 0.04, n = 7), whereas CPZ, FFA, NL, and βOG significantly decreased ENaC activity ($I_{sub}/I_{ami}$: CPZ: 0.87 ± 0.02, n = 10; FFA: 0.95 ± 0.006, n = 8; NL: 0.77 ± 0.03, n = 8; βOG: 0.77 ± 0.03, n = 8). This sensitivity to amphiphilic molecules is in line with a previous report, showing that ENaC is sensitive to CPZ, which probably acts via the membrane environment on ENaC (17). Taken together, these data suggest that 1) the amphiphilic compounds may act nonspecifically and 2) that amphiphile sensitivity is possibly a general feature of DEG/ENaCs. Nevertheless, these results do not exclude specific effects of some amphiphilic substances on the channels.

## gA is similarly affected by amphiphilic substances

gA is an amphiphilic pore-forming peptide with antibiotic potential. Gramicidin channels are dimers formed by the transbilayer association of monomeric subunits from each leaflet (43). Based on these properties, gA was proposed to serve as a molecular force probe, allowing the prediction of membrane perturbation by compounds (44). Here, we made use of gA to test whether the amphiphilic substances at the concentrations we used for ion channel modulation in *Xenopus* oocytes have the potential to alter membrane properties. gA was applied at a concentration of 40 μM to uninjected oocytes for 8 min. Directly after the application of gA, an inward current was triggered, which continuously increased over minutes (Fig. 7 *A*). After 8 min, the amphiphilic substance was applied for 3 min. NL significantly increased the gA current ($I_{+subst}/I_{-subst}$, NL: 5.48 ± 1, n = 9; βOG: 1.55 ± 0.16 n = 7), whereas FFA, CPZ, and CAP decreased the gA current ($I_{+subst}/I_{-subst}$, FFA: 0.47 ± 0.06, n = 8; CPZ: 0.69 ± 0.02, n = 6; CAP: 0.72 ± 0.05, n = 7) (Fig. 7, *A* and *B*). Taken together, these results suggest that these amphiphilic substances indeed modified the physical properties of the *Xenopus* oocyte membrane, which affected the formation of gA channels. However, specific interactions between gA and the various substances tested cannot be fully ruled out.

## Effect of channel-modifying amphiphilic substances in model lipid membranes

Because the observed effects of amphiphilic substances on DEG/ENaCs may be due to unspecific membrane modulation, we analyzed the effect of the amphiphilic substances on lipid membranes using oriented, synthetic bilayers. Two-dimensional x-ray intensity maps were obtained for membrane samples prepared with the amphiphilic molecules. All molecules were found to partition into the bilayer and significantly influence bilayer properties. We first illustrate in detail the membrane effects caused by two specific cases (i.e., FFA and CPZ) and then present a summary for all molecules in this study.

CPZ and FFA induce unique changes to bilayer structure, as highlighted in Fig. 8. Out-of-plane reflectivities for membranes with 0, 3, and 10 mol% FFA (relative number of moles in membrane) are shown in Fig. 8 *A*. Whereas 0 and 3 mol% samples have evenly spaced Bragg peaks, indicative of a lamellar structure, 10 mol% shows additional peaks that are not well indexed by a single lamellar phase. These peaks are best described by a three-dimensional cubic phase structure with a side length of 136 Å (28). Cubic phases in lipid systems are observed typically when lipids and surfactants induce high-negative curvature into the bilayers (28,45,46). As illustrated in Fig. 8 *B*, the isotropic scattering along the ring Q ~0.11 $Å^{-1}$ is the signature of the formation of a highly bent cubic phase (the cubic (211) peak).

On solid support, the DMPC membranes typically exist in the lamellar phase (28,29,31). To determine how FFA causes curvature leading to a cubic phase, the electron density profile of the bilayers with 3 mol% FFA, which was still in the lamellar phase, was compared to that of pure DMPC bilayers (Fig. 8 *C*). Differences in electron density between FFA 3 and 0 mol% reveal the location of FFA in the bilayer. Changes in density are observed in both the head group and tail group regions. As shown in Fig. 8 *C*, there is increased density in the tail group region ($z < 16$ Å) and decreased density in the lipid head groups ($z > 16$ Å). The increased tail density indicates that FFA partitions into the tail region and increases density in the hydrophobic core, causing the increase in curvature. The common analgesic ibuprofen was recently reported to interact with lipid tails, causing cubic phases and significant curvature stress (28). We propose that, similarly to ibuprofen, FFA also induces negative curvature by increasing volume in the lipid tails, leading to cubic phases at high concentrations.

CPZ has a different effect on the DMPC bilayers. Out-of-plane reflectivities for membranes with 0, 3, and 10 mol%

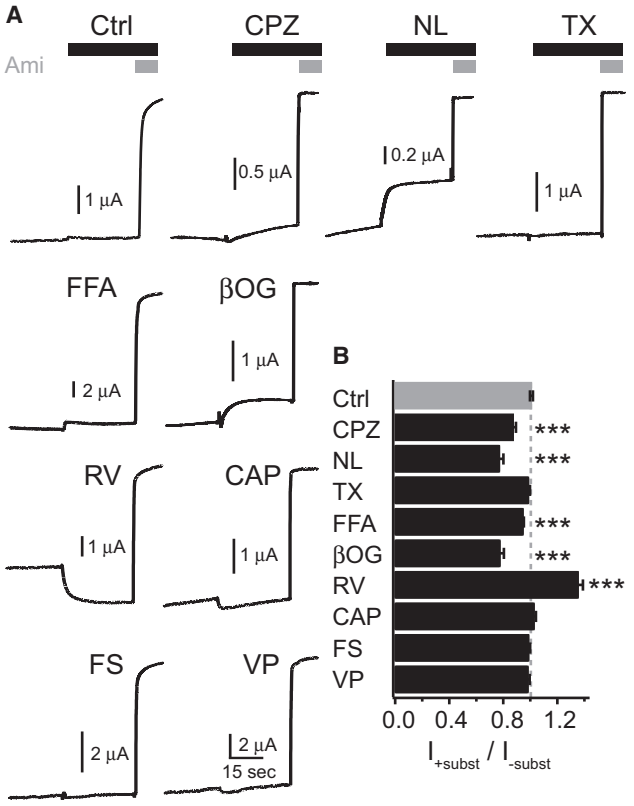


FIGURE 6 rENaC is modulated by the amphiphilic substances. (*A*) Current recordings of representative oocytes expressing r$\alpha\beta\gamma$ENaC are shown. Bath solutions were supplemented with vehicle (DMSO) (Ctrl), 250 $\mu$M CPZ, 500 $\mu$M NL, 100 $\mu$M TX, 1 mM FFA, 5 mM $\beta$OG, 100 $\mu$M RV, 250 $\mu$M CAP, 1 mM FS, or 1 mM VP (*black bar*). Amiloride-sensitive currents were determined by block with 10 $\mu$M amiloride (Ami, *gray bar*). (*B*) Quantitative analysis of the mean amiloride-sensitive currents in the presence of the substances relative to the amiloride-sensitive current before substance application. The mean amiloride-sensitive current ranged from $-16.3 \pm 1.4$ to $-1.7 \pm 0.4$ $\mu$A (control $-8.3 \pm 1.5$ $\mu$A, n = 7–24). Bars represent the mean, and the error bars the mean $\pm$ SE (n = 7–24, $*p < 0.05$, $**p < 0.01$, $***p < 0.001$).

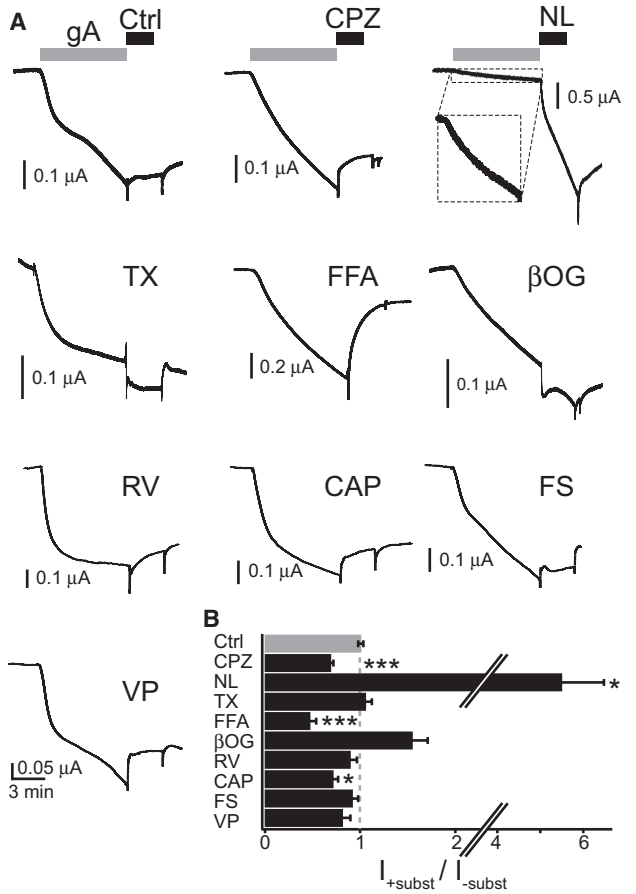


FIGURE 7 Gramicidin A responds to the amphiphilic compounds. (*A*) Representative current traces of native oocytes exposed to 40 $\mu$M gA (*gray bars*) for 8 min are shown. The testing solutions (*black bars*) were supplemented with vehicle (Ctrl), 250 $\mu$M CPZ, 500 $\mu$M NL, 100 $\mu$M TX, 1 mM FFA, 5 mM $\beta$OG, 100 $\mu$M RV, 250 $\mu$M CAP, 1 mM FS, or 1 mM VP. (*B*) Relative currents mediated by gA in the presence of the substance relative to the current evoked by gA alone. The gA-induced current ranged from $-0.9 \pm 0.2$ to $-0.2 \pm 0.07$ $\mu$A (control $-0.7 \pm 0.1$ $\mu$A, n = 6–25). Bars represent the mean, and the error bars represent the mean $\pm$ SE (n = 6–25, $*p < 0.05$, $**p < 0.01$, $***p < 0.001$).

CPZ are shown in Fig. 8 *D*. At 10 mol%, the set of Bragg peaks are also not indexed by a single lamellar phase. However, the pattern is not indicative of a cubic phase. Instead, these peaks are indexed by coexisting lamellar phases, as previously observed for bilayers with melatonin (37). Whereas $d_z = 55$ Å for the first lamellar phase, the second lamellar phase has a much smaller spacing of 43 Å. The smaller lamellar spacing further decreases to 42 Å at 10 mol% CPZ, indicating that CPZ is inducing a thinner membrane phase. The decreased $d_z$ indicates a significant increase in lipid fluidity (29–32). The bilayers containing CPZ do not display the same degree of bending, as illustrated by the 10 mol% sample in Fig. 8 *E*. The electron density profile for the 3 mol% CPZ bilayer, which is in a single lamellar phase, is compared to a DMPC bilayer in Fig. 8 *F*. Relative to DMPC, there is a clear increase in density in the head groups but also in the tail groups. The relative increase in density for the head and tail regions is calculated by integrating the density difference between the curves from $d_z < z < d_C$ (for the heads) and $d_C < z < 0$ (for the tails) and taking the ratio. The results are displayed in Fig. 8 *F*. A large increase in density in the head groups in addition to a minor increase in the tails can be observed. Molecules such as aspirin and melatonin have been observed in the lipid head groups, leading to similar drastic decreases in $d_z$ (31,32). The position of the CPZ molecule is assigned to the head group density, whereas the extra density in the tails is either a result of a second CPZ position or, more likely, due to an increased tail density due to the decrease in $d_z$ (1 Å) between 0 and 3 mol% CPZ.

The results present a clear dichotomy between how CPZ and FFA interact with lipid membranes. Whereas FFA interacts with the lipid tails and induces strong curvature stress, which eventually leads to the formation of a cubic phase,

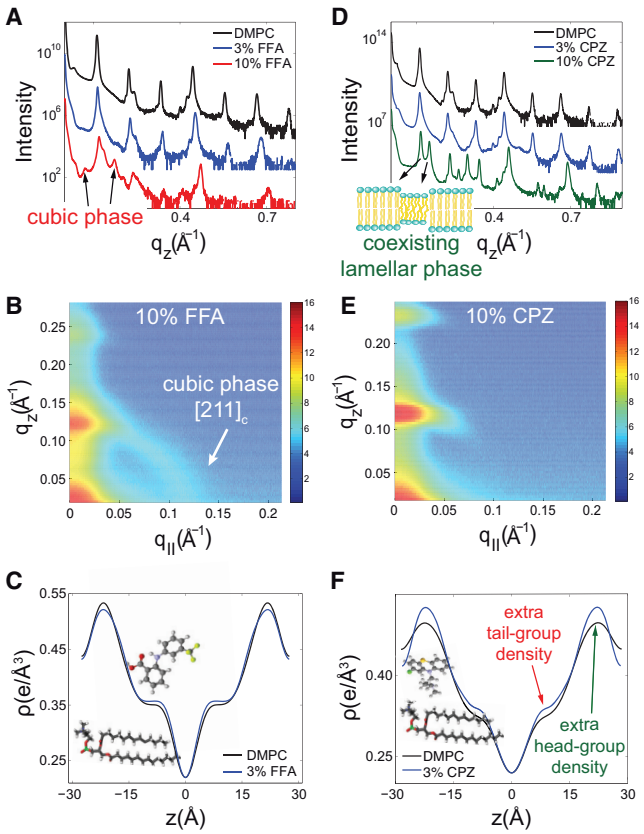


FIGURE 8 Detailed analysis for model membrane samples containing FFA and CPZ. (*A*) Out-of-plane x-ray reflectivities for samples with 0, 3, and 10 mol% FFA. (*B*) High-resolution RSM for 10 mol% FFA, showing the formation of a highly bent cubic phase. (*C*) Electron density profiles for 0 and 3 mol% FFA. (*D*) Reflectivities for 0, 3, and 10 mol% CPZ are shown. (*E*) High-resolution RSM for 10 mol% CPZ, indicating membrane bending but no cubic phase, as with 10 mol% FFA. (*F*) Electron density profiles for 0 and 3 mol% CPZ are shown.

CPZ interacts primarily with the lipid head groups, causing significant decreases in bilayer spacing and increases in fluidity.

For all molecules in the study, the change in membrane structure, added curvature stress, and relative increase in head and tail density caused by the molecules were calculated (Fig. 9). βOG, similarly to FFA, primarily causes increases in tail density and induces highly bent cubic phases. NL and TX cause comparable increases in density in both the heads and the tails, with the tail groups being slightly denser. The tail group density is enough to cause increased curvature stress, as observed in the orientation plots (Fig. 9). NL and TX can, therefore, be speculated to interact with both lipid heads and tails. FS shows the smallest partitioning coefficient (0.036, approximately 10 times smaller than all other molecules) of all molecules investigated and is weakly interacting only with the bilayers. RV and CAP mainly increase density in the head group region; however, they also lead to membrane thinning and increased bending. VP shows a stronger presence in the tail group region with membrane thinning and significant bending (Fig. 9). An estimation of the partitioning coefficients of the amphiphilic substances and their concentrations in the membranes revealed that in both experimental approaches they were in similar ranges (Table 1).

Qualitatively, increased tail group interaction is associated with increased membrane bending. Conversely, increased head group density is associated with limited bending and decreased bilayer spacing, indicative of increases in lipid fluidity. In summary, all molecules analyzed in this study significantly impact lipid bilayer properties.

## Structural analysis of cASIC1 and zP2X4

As amphiphilic compounds changed membrane properties, we hypothesized that these changes could modulate DEG/ENaCs by favoring certain conformations, thereby shifting the equilibrium between conducting and nonconducting conformations. The shift in conformational equilibrium in response to altered lipid bilayer properties is believed to arise mainly from shape changes of transmembrane segments during conformational transitions (47). Different measures for the shape of TMDs were previously used, e.g., the cross-sectional area profile or the shape of the ion pore (48,49). In the case of cASIC1, the fenestrated nature of its TMDs (Fig. 10 *A*, fenestrations highlighted in *blue*) hindered the precise determination of the cross-sectional area profile. Therefore, we instead determined the average cross-sectional diameter profile of cASIC1 in the open and desensitized state (see Materials and Methods; (50,51)). The average cross-sectional diameter profile is not affected by the presence of a fenestrated TMD because its calculation does not require a completely defined protein-lipid boundary, and yet it provides an overview on the lateral expansion of the protein within the lipid bilayer. The structure of the closed state, which would have been an ideal reference point, is not available. Thus, the changes in the cross-sectional diameter profile described here have to be considered as an approximation to possible structural changes during gating.

According to the analysis of the cross-sectional diameter profile, the largest spatial differences between the open and the desensitized state of cASIC1 and hence the largest molecular movements and lateral expansions were observed in the TMDs and the ECD adjacent to the TMDs (Fig. 10, *A–C*).

We performed a similar analysis of an ATP-gated P2X receptor that is not directly related to DEG/ENaCs but has a similar topology, with two TMDs, a large ECD, and intracellular N- and C-termini. Moreover, P2X receptors share a trimeric composition and overall structure with ASICs (52). We measured the spatial expansion of zebrafish P2X4, for which high-resolution structures of the closed and the open conformations are available (53). Similar to cASIC1,

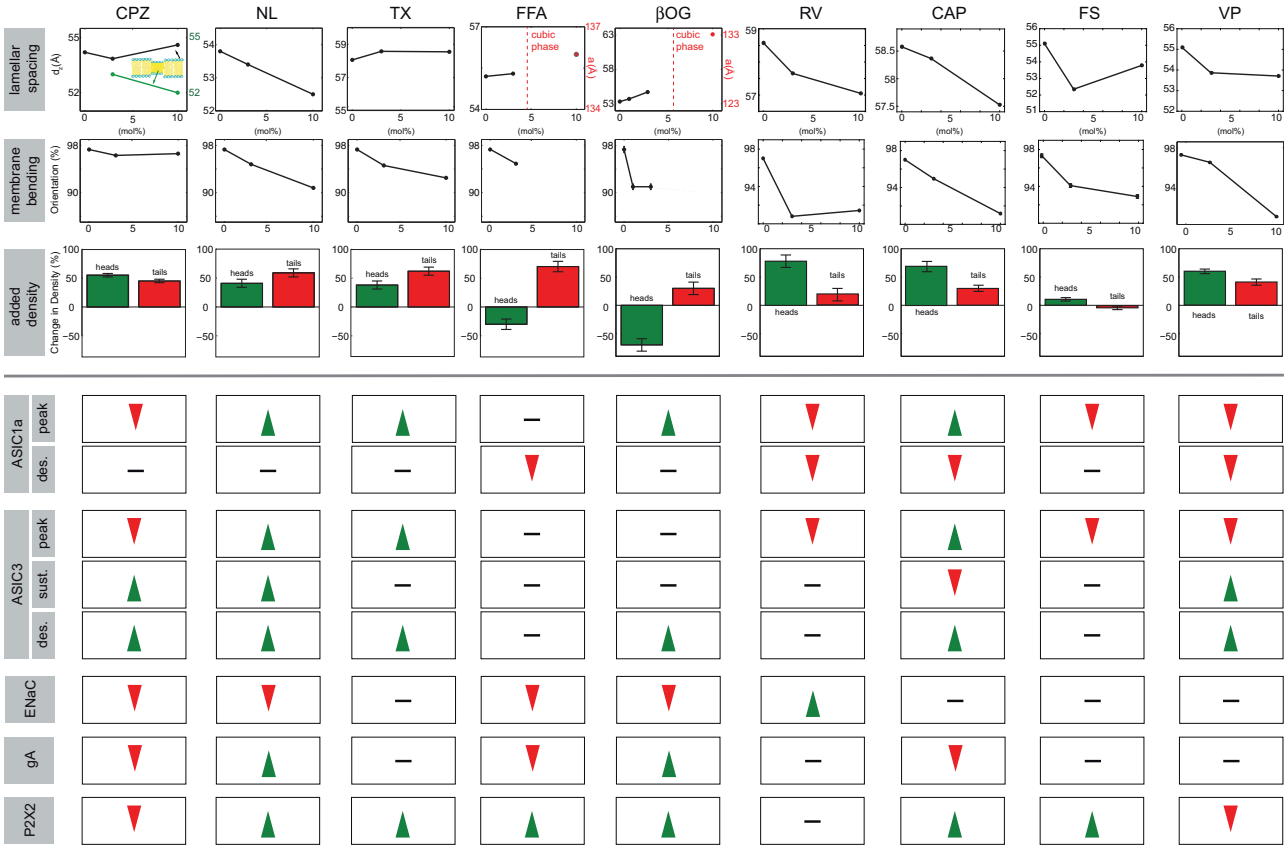


FIGURE 9 A table of charts summarizing the effects of the amphiphilic molecules on DMPC membranes and on ion channels properties. Rows describe the changes to lamellar spacing and/or structure caused by the amphiphilic molecules, the change in bending, and the relative added electron density to the heads and tails caused by the molecules. The following rows summarize the significant effects of the amphiphilic molecules on peak amplitude and desensitization of rASIC1a, the effect on peak amplitude, the sustained current amplitude and desensitization of rASIC3, the effect on ATP-induced rP2X2 current amplitude, the effect on amiloride-sensitive ENaC current, and the effect on gA activity (*green arrow* = increase, *red arrow* = decrease). The columns are organized by molecules studied. Note that for $d_z$ and orientation, error bars are smaller than the size of the marks (<1%).

the largest spatial movements of P2X4 occurred in the TMDs and the region above these domains (Fig. 10, *D–F*). If our hypothesis is true, these similar shape changes will predict that P2X receptors are also sensitive to amphiphilic substances.

To test this prediction, we performed electrophysiological recordings of rP2X2, the primary amino acid sequence of which is 37% identical to zP2X4. rP2X2 was repetitively activated with 5 $\mu$M ATP, and amphiphilic substances were applied 10 s before and during ATP-induced activation. In line with our prediction, the amphiphilic substances strongly affected rP2X2 responses to ATP. Overall, amphiphilic substances had more dramatic effects on rP2X2 than on ASICs (Fig. 11, *A* and *B*). Compared to control measurements ($I_{peak/+sub.}/I_{peak/-sub.}$: control: 0.92 ± 0.025, n = 19), NL and $\beta$OG increased rP2X2 currents most potently ($I_{peak/+sub.}/I_{peak/-sub.}$: 6.86 ± 0.64 and 11.36 ± 1.62-fold, n = 7 and n = 11), respectively, whereas FFA and TX increased rP2X2 currents ~threefold (3.66 ± 0.48-fold and 3.34 ± 0.38-fold; n = 12–15). CAP had the weakest effect (1.47 ± 0.16-fold, n = 17). Similar to rASIC1a, CPZ and VP decreased the rP2X2 current approximately by a factor of ~2 ($I_{peak/+sub.}/I_{peak/-sub.}$: CPZ: 0.54 ± 0.05, n = 7; VP: 0.45 ± 0.03, n =7–12).

Similar to rASIC3, we determined the ATP affinity of rP2X2 in the presence and absence of the two amphiphilic substances $\beta$OG and CPZ. $\beta$OG shifted the affinity for ATP from $EC_{50}$ 44.7 ± 8.9 to 17.7 ± 4.2 $\mu$M ($p < 0.001$, n = 10), whereas CPZ did not affect ATP affinity (Fig. 11, *C* and *D*).

Taken together, these results suggest that P2X receptors are also sensitive to amphiphilic substances and possibly membrane alterations. In addition, they suggest that analysis of the conformational changes of the TMDs of ion channels during gating may help to predict sensitivity to amphiphile substances.

## DISCUSSION

In this study, we report that a selection of structurally unrelated amphiphilic molecules affect the DEG/ENaCs rASIC1a, rASIC3, and rENaC. All molecules showed

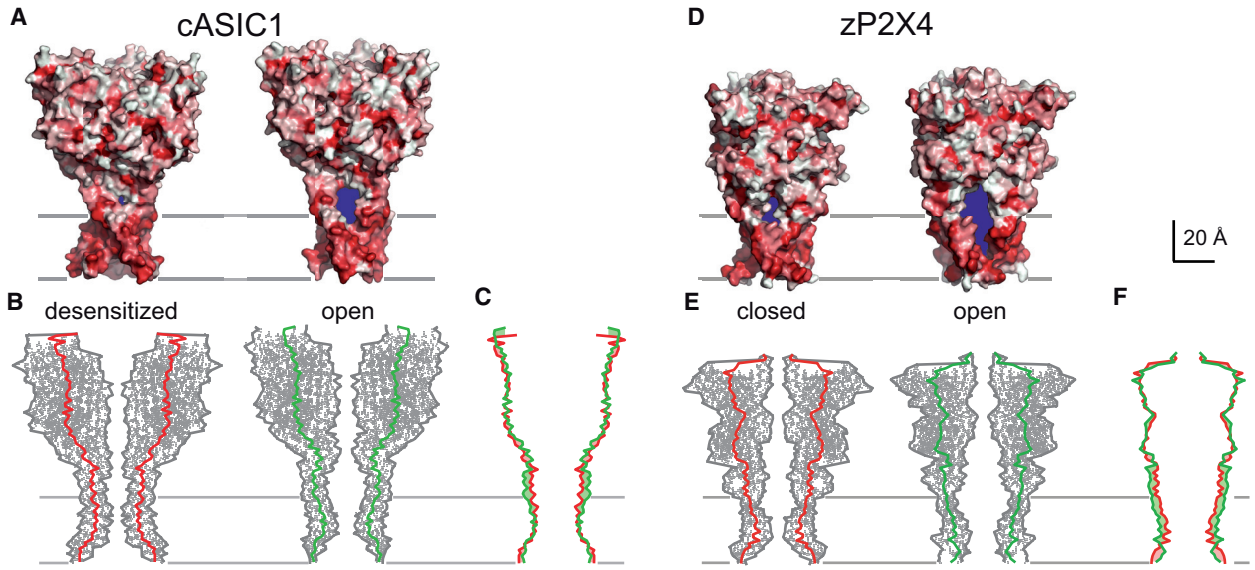


FIGURE 10 Shape changes in the transmembrane domains during gating of cASIC1 and zP2X4. (*A* and *B*) Representations of cASIC1 crystal structures of the desensitized (*left*, PDB: 4NYK) and open (*right*, PDB: 4NTW) conformation in relation to the plasma membrane (indicated in *gray*). (*A*) The solvent-excluded surface area adequate for lipid tail groups (solvent radius set to 2Å) is displayed and color-coded according to the residue hydrophobicity (*white* is hydrophilic, *red* is hydrophobic). Fenestrations connecting the ion pore and the membrane or aqueous environment are highlighted in blue. (*B*) Shown are cross-sectional diameter profiles of both channel conformations, in which atom distance with regard to the central channel axis is plotted horizontally, and atom position alongside the central channel axis is plotted vertically. Dots represent single atoms, colored lines represent average cross-sectional diameters, and gray lines represent cross-sectional diameter maxima and minima. For clarity, the plots are mirrored at the central channel axis and averages, and minima and maxima were calculated for 1.5 Å increments. (*C*) Shown is a comparison of average cross-sectional diameters of the desensitized and open state taken from (*B*) and color-coded accordingly. (*D–F*) Representations of zP2X4 crystal structures of the closed (*left*, PDB: 4DW0) and open (*right*, PDB: 4DW1) conformation are shown in relation to the plasma membrane and their comparison (as for *A–C*).

potential to modify ion channel activity; the observed effects, however, varied for amphiphilic molecules and ion channels. For example, TX and NL both increased rASIC1a and rASIC3 current amplitudes, whereas only NL decreased ENaC current. (Figs. 3, 4, and 5). $\beta$OG, on the other hand, potently increased rASIC1a currents but showed no significant effect on rASIC3 (Figs. 3, 4, and 5). Other substances like RV, CAP, FS, and VP showed similar effect on rASIC1a and rASIC3 but did not act or acted differently on ENaC (Fig. 6). In addition to changes in current amplitude, the kinetic of rASIC1a and rASIC3 desensitization was also altered by some but not all of the molecules included in this study (Figs. 3 and 5). Furthermore, the transient and the sustained current of rASIC3 were in part affected differently. CAP, for example, increased the transient but decreased the sustained current, whereas CPZ decreased transient but increased sustained rASIC3 currents (Fig. 5). Taken together, the extent of channel modification induced by amphiphilic molecules was variable and dependent on the channel tested. Changes of the current amplitude as well as desensitization kinetics by amphiphilic compounds suggest that they influenced both the equilibrium between closed and open conformations as well as between open and desensitized conformations. As a mechanistic basis of the modulation, either a nonspecific membrane modulation or a direct interaction of the amphiphilic substances with the channels is conceivable.

Amphiphilic molecules had either no effect on or inhibited rENaC, and only RV increased ENaC currents (Fig. 6). ENaC is a constitutively active channel, which undergoes slow closed-open transitions (54). It exists in either a mode with a high open probability ($P_o$) or with a low (near silent) $P_o$ (55). It appears that mainly the high-$P_o$ mode is sensitive to amphiphilic molecules, which might explain why these had mostly inhibitory effects on ENaC.

We assessed the membrane-modulating potential of the amphiphilic substances by testing their effect on gA activity. Four amphiphilic molecules studied indeed influenced gA activity (Fig. 7). This shows that these amphiphilic molecules affect membrane properties at the concentrations used to study DEG/ENaCs. In agreement, in the x-ray scattering approach, which allowed determination of the localization of the molecules within the lipid bilayer and analysis of membrane bending and lamellar spacing, all molecules analyzed accumulated in the lipid bilayer and affected membrane properties differently (Figs. 8 and 9). The concentration of amphiphilic substances in the membranes were similar (within a factor of 3.5) between both experimental approaches, with the exception of $\beta$OG, in which the concentration was >10-fold higher in the electrophysiological experiments (Table 1). Less hydrophobic molecules such as CPZ interact more strongly with head groups and decrease membrane spacing, whereas hydrophobic molecules such as FFA and $\beta$OG interact with tail groups and

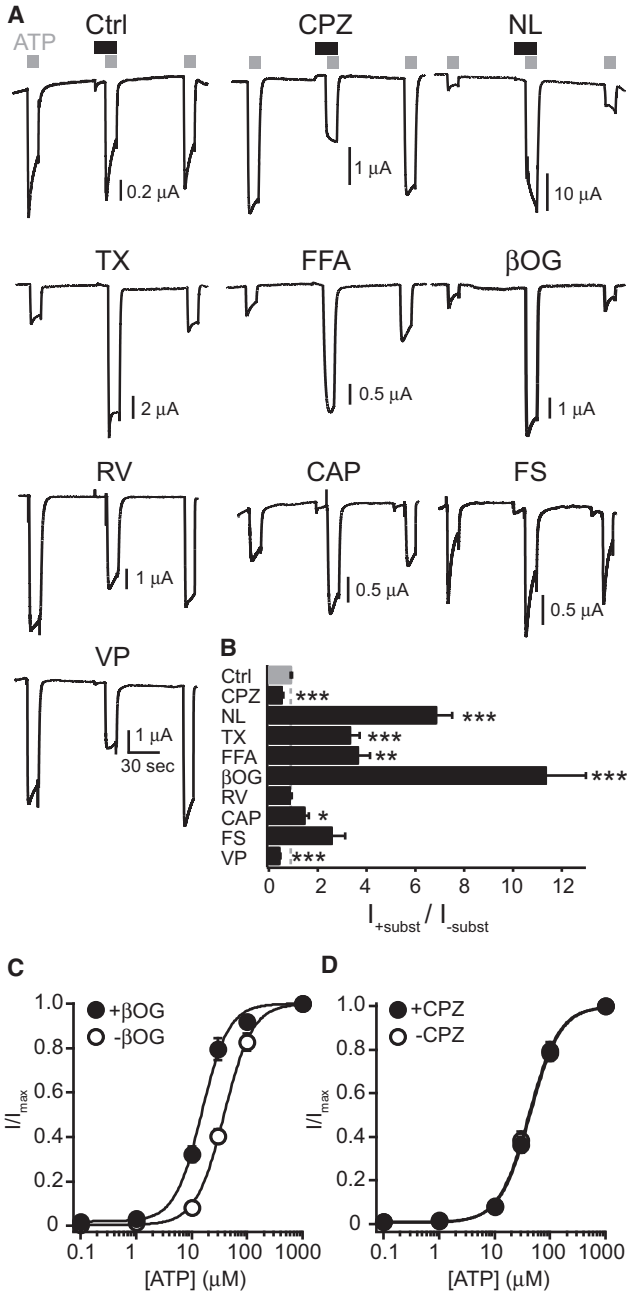


FIGURE 11 The purinergic receptor rP2X2 is modulated by amphiphilic compounds. (*A*) Representative current traces of oocytes expressing rP2X2, repetitively activated by 5 $\mu$M ATP (*gray bars*) alone or combined with the pre- and coapplication of an amphiphilic substance. No substance (Ctrl), 250 $\mu$M CPZ, 500 $\mu$M NL, 100 $\mu$M TX, 1 mM FFA, 5 mM $\beta$OG, 100 $\mu$M RV, 250 $\mu$M CAP, 1 mM FS, or 1 mM VP was added to the bath solutions during the period indicated by the black bars. (*B*) Quantitative analysis of the ATP-induced peak currents in the presence of the substances was normalized to the previous ATP-induced activation in their absence. The mean amplitude of the first activation ranged from $-7.8 \pm 2.8$ to $-1.2 \pm 0.2$ $\mu$A (control $-3.6 \pm 1.7$ $\mu$A, n = 7–19). Bars represent the mean, and the error bars represent the mean $\pm$ SE (n = 7–19, * $< 0.05$, ** $p < 0.01$, *** $p < 0.001$). (*C*) ATP concentration-response curves for rP2X2 in the absence (*open circle*) and presence (*closed circles*) of 5 mM $\beta$OG. (*D*) ATP concentration-response curves for rP2X2 in the absence (*open circle*) and presence (*closed circles*) of 250 $\mu$M CPZ. Currents were normalized to the maximal activation at 1 mM ATP. Lines represent fits to the Hill equation. Error bars represent the mean $\pm$ SE (n = 10).

cause membrane curvature and eventually the formation of highly bent cubic phases. Therefore, the molecules have differential impacts on both membrane structure and channel activity.

Although we cannot fully exclude specific interactions of the amphiphilic substances with the different ion channels, we suggest that their interaction with the membrane plays a role in their impact on channel activity. It is believed that membrane proteins become sensitive to alterations of membrane properties when relevant conformational changes involve the domains interacting with the membrane (47). To test if this applies to cASIC1, we inspected in detail the structure of cASIC1 in the desensitized and the open conformation. Unfortunately, the closed conformation of a cASIC1 has not been reported yet; therefore, we can only examine conformational dynamics during the open-to-desensitized transition. We measured the cross-sectional diameter profile of the channel and observed that the maximal lateral expansion changes indeed occur within the TMDs and the region slightly above the TMDs (Fig. 10). This is in agreement with previous reports (50,56,57) and represents a possible molecular mechanism for sensitivity to membrane alterations and amphiphilic substances.

To test whether other channels might be similarly affected by amphiphilic molecules, we used an unrelated channel. We analyzed the zP2X4 receptor in the open and the closed conformation using an identical approach as described for cASIC1 and identified the TMDs as the region in which the largest changes of the cross-sectional diameter occur (Fig. 10), showing that large conformational changes in the TMDs also occur during the closed-to-open transition in a channel with a structure similar to that of DEG/ENaCs. Moreover, rP2X2 indeed showed a high degree of susceptibility to the same amphiphilic molecules (Fig. 11) as those of DEG/ENaCs and gA. This finding is in agreement with our hypothesis that when large conformational changes in the TMDs occur, an ion channel may be sensitive to changes in its membrane environment.

A clear correlation between membrane activity, as measured with the model membrane experiments, and effects on channel activity was not observed (Fig. 9). Future experiments need to target each channel individually to build a detailed model of how the membrane environment influences channel activity. A specific ion channel could be sensitive to a variety of membrane properties like the lateral pressure profile of the bilayer, hydrophobic matching, areal deformation, Gaussian curvature, or a combination of the above (27,58).

We have shown that DEG/ENaCs are modulated by amphiphilic molecules and propose that this modulation may at least be partly due to alterations of plasma membrane

properties. We suggest that DEG/ENaCs have a certain degree of membrane sensitivity in common. This concept of membrane sensitivity is based on the following results: 1) structurally different molecules have similar effects; 2) various DEG/ENaCs are affected by amphiphilic molecules; 3) amphiphilic molecules modulate gA, suggesting changes in membrane properties; 4) the largest lateral expansions of cASIC1a during gating occur in the TMD; 5) structural analysis of P2X channels predicts membrane sensitivity; 6) rP2X2 is highly sensitive to the same amphiphilic compounds, which modify DEG/ENaCs and gA; and 7) at least four of the amphiphilic substances used in this study have previously been shown to affect some ion channels via membrane-mediated mechanisms (24,25). Nevertheless, all of the observed effects may, in principle, also be explained by specific interaction with the channels.

A recent study showed that ASIC1a activity is increased by the presence of the bile acid known as deoxycholic acid (59). Based on a molecular docking approach and site-directed mutagenesis, the authors proposed a binding site for bile acids within the pore region of the channel in close proximity to the degenerin site. A similar finding was reported for ENaCs by the same authors (60). Our finding that structurally unrelated molecules have similar effects on channel activity renders a single binding site for all these compounds unlikely. We cannot, however, exclude that such a binding site exists for some of the compounds, which mediates part of their effect. ASIC3 has been linked to mechanotransduction (10–12) and lipid signaling (61), two findings that are in line with the conclusion that the plasma membrane might play a regulatory role for ASIC3.

### Pharmacological relevance

A lot of progress has been made in recent years on the physiology of DEG/ENaCs, in particular with regard to ASICs and their pharmacological manipulation. The importance of physiological processes like signal transmission or pain sensation makes ASICs interesting pharmacological targets. Especially for the development of new agonists and antagonists, we think it is important to understand the role of the plasma membrane in the activity of the channel. Newly developed drugs should be tested for modulation of the plasma membrane, as this may contribute to putative off-target effects.

In summary, our study shows that DEG/ENaCs are susceptible to amphiphilic substances and therefore possibly to their membrane environment. This may be helpful to evaluate specific molecules targeting members of the DEG/ENaC family and also other channels.

## AUTHOR CONTRIBUTIONS

A.S. and R.J.A. designed and performed research, analyzed data, and wrote the manuscript. R.R., P.L., S.J., A.K., and N.N.G. performed research. S.G., M.C.R., and D.W. designed research, analyzed data, and wrote the manuscript.

## ACKNOWLEDGMENTS

The authors thank A. Oslender-Bujotzek for expert technical assistance.

## REFERENCES

1. Kellenberger, S., and L. Schild. 2002. Epithelial sodium channel/degenerin family of ion channels: a variety of functions for a shared structure. *Physiol. Rev.* 82:735–767.
2. Kellenberger, S., and L. Schild. 2015. International Union of Basic and Clinical Pharmacology. XCI. structure, function, and pharmacology of acid-sensing ion channels and the epithelial Na+ channel. *Pharmacol. Rev.* 67:1–35.
3. Jasti, J., H. Furukawa, …, E. Gouaux. 2007. Structure of acid-sensing ion channel 1 at 1.9 A resolution and low pH. *Nature.* 449:316–323.
4. Wiemuth, D., M. Assmann, and S. Gründer. 2014. The bile acid-sensitive ion channel (BASIC), the ignored cousin of ASICs and ENaC. *Channels (Austin).* 8:29–34.
5. Waldmann, R., G. Champigny, …, M. Lazdunski. 1997. A proton-gated cation channel involved in acid-sensing. *Nature.* 386:173–177.
6. Arias, R. L., M.-L. A. Sung, …, M. Monaghan. 2008. Amiloride is neuroprotective in an MPTP model of Parkinson's disease. *Neurobiol. Dis.* 31:334–341.
7. Friese, M. A., M. J. Craner, …, L. Fugger. 2007. Acid-sensing ion channel-1 contributes to axonal degeneration in autoimmune inflammation of the central nervous system. *Nat. Med.* 13:1483–1489.
8. Xiong, Z. G., X. M. Zhu, …, R. P. Simon. 2004. Neuroprotection in ischemia: blocking calcium-permeable acid-sensing ion channels. *Cell.* 118:687–698.
9. Chalfie, M. 2009. Neurosensory mechanotransduction. *Nat. Rev. Mol. Cell Biol.* 10:44–52.
10. Chen, C. C., and C. W. Wong. 2013. Neurosensory mechanotransduction through acid-sensing ion channels. *J. Cell. Mol. Med.* 17:337–349.
11. Jalalvand, E., B. Robertson, …, S. Grillner. 2016. Ciliated neurons lining the central canal sense both fluid movement and pH through ASIC3. *Nat. Commun.* 7:10002.
12. Lin, S. H., Y. R. Cheng, …, C. C. Chen. 2016. Evidence for the involvement of ASIC3 in sensory mechanotransduction in proprioceptors. *Nat. Commun.* 7:11460.
13. Chen, C. C., A. Zimmer, …, A. Zimmer. 2002. A role for ASIC3 in the modulation of high-intensity pain stimuli. *Proc. Natl. Acad. Sci. USA.* 99:8992–8997.
14. Deval, E., J. Noël, …, E. Lingueglia. 2008. ASIC3, a sensor of acidic and primary inflammatory pain. *EMBO J.* 27:3047–3055.
15. Boscardin, E., O. Alijevic, …, S. Kellenberger. 2016. The function and regulation of acid-sensing ion channels (ASICs) and the epithelial Na(+) channel (ENaC): IUPHAR Review 19. *Br. J. Pharmacol.* 173:2671–2701.
16. Schmidt, A., P. Lenzig, …, D. Wiemuth. 2014. The bile acid-sensitive ion channel (BASIC) is activated by alterations of its membrane environment. *PLoS One.* 9:e111549.
17. Awayda, M. S., W. Shao, …, W. G. Hill. 2004. ENaC-membrane interactions: regulation of channel activity by membrane order. *J. Gen. Physiol.* 123:709–727.
18. Kawate, T., J. C. Michel, …, E. Gouaux. 2009. Crystal structure of the ATP-gated P2X(4) ion channel in the closed state. *Nature.* 460:592–598.
19. Burnstock, G., B. B. Fredholm, …, A. Verkhratsky. 2010. The birth and postnatal development of purinergic signalling. *Acta Physiol. (Oxf.).* 199:93–147.
20. Gonnord, P., C. Delarasse, …, J. M. Kanellopoulos. 2009. Palmitoylation of the P2X7 receptor, an ATP-gated channel, controls its expression and association with lipid rafts. *FASEB J.* 23:795–805.
21. Allsopp, R. C., U. Lalo, and R. J. Evans. 2010. Lipid raft association and cholesterol sensitivity of P2X1-4 receptors for ATP: chimeras

and point mutants identify intracellular amino-terminal residues involved in lipid regulation of P2X1 receptors. *J. Biol. Chem.* 285:32770–32777.

22. Robinson, L. E., M. Shridar, …, R. D. Murrell-Lagnado. 2014. Plasma membrane cholesterol as a regulator of human and rodent P2X7 receptor activation and sensitization. *J. Biol. Chem.* 289:31983–31994.
23. Bernier, L. P., A. R. Ase, …, P. Séguéla. 2008. Phosphoinositides regulate P2X4 ATP-gated channels through direct interactions. *J. Neurosci.* 28:12938–12945.
24. Lundbaek, J. A., P. Birn, …, O. S. Andersen. 2004. Regulation of sodium channel function by bilayer elasticity: the importance of hydrophobic coupling. Effects of Micelle-forming amphiphiles and cholesterol. *J. Gen. Physiol.* 123:599–621.
25. Ingólfsson, H. I., P. Thakur, …, O. S. Andersen. 2014. Phytochemicals perturb membranes and promiscuously alter protein function. *ACS Chem. Biol.* 9:1788–1798.
26. Andersen, O. S., and R. E. Koeppe, 2nd. 2007. Bilayer thickness and membrane protein function: an energetic perspective. *Annu. Rev. Biophys. Biomol. Struct.* 36:107–130.
27. Lundbaek, J. A. 2008. Lipid bilayer-mediated regulation of ion channel function by amphiphilic drugs. *J. Gen. Physiol.* 131:421–429.
28. Alsop, R. J., C. L. Armstrong, …, M. C. Rheinstädter. 2015. Cholesterol expels ibuprofen from the hydrophobic membrane core and stabilizes lamellar phases in lipid membranes containing ibuprofen. *Soft Matter.* 11:4756–4767.
29. Alsop, R. J., M. A. Barrett, …, M. C. Rheinstädter. 2014. Acetylsalicylic acid (ASA) increases the solubility of cholesterol when incorporated in lipid membranes. *Soft Matter.* 10:4275–4286.
30. Alsop, R. J., A. Khondker, …, M. C. Rheinstädter. 2016. The lipid bilayer provides a site for cortisone crystallization at high cortisone concentrations. *Sci. Rep.* 6:22425.
31. Barrett, M. A., S. Zheng, …, M. C. Rheinstädter. 2012. Interaction of aspirin (acetylsalicylic acid) with lipid membranes. *PLoS One.* 7:e34357.
32. Dies, H., B. Cheung, …, M. C. Rheinstädter. 2015. The organization of melatonin in lipid membranes. *Biochim. Biophys. Acta.* 1848:1032–1040.
33. Wiemuth, D., and S. Gründer. 2010. A single amino acid tunes Ca2+ inhibition of brain liver intestine Na+ channel (BLINaC). *J. Biol. Chem.* 285:30404–30410.
34. Madeja, M., U. Musshoff, and E. J. Speckmann. 1995. Improvement and testing of a concentration-clamp system for oocytes of Xenopus laevis. *J. Neurosci. Methods.* 63:211–213.
35. Chen, X., M. Paukert, …, S. Gründer. 2006. Strong modulation by RFamide neuropeptides of the ASIC1b/3 heteromer in competition with extracellular calcium. *Neuropharmacology.* 50:964–974.
36. Dies, H., L. Toppozini, and M. C. Rheinstädter. 2014. The interaction between amyloid-β peptides and anionic lipid membranes containing cholesterol and melatonin. *PLoS One.* 9:e99124.
37. Tang, J., R. J. Alsop, …, M. C. Rheinstädter. 2016. Amyloid-β(25-35) peptides aggregate into cross-β sheets in unsaturated anionic lipid membranes at high peptide concentrations. *Soft Matter.* 12:3165–3176.
38. Vasilets, L. A., G. Schmalzing, …, W. Schwarz. 1990. Activation of protein kinase C by phorbol ester induces downregulation of the Na+/K(+)-ATPase in oocytes of Xenopus laevis. *J. Membr. Biol.* 118:131–142.
39. Sigel, E. 1990. Use of Xenopus oocytes for the functional expression of plasma membrane proteins. *J. Membr. Biol.* 117:201–221.
40. Kučerka, N., M. P. Nieh, and J. Katsaras. 2011. Fluid phase lipid areas and bilayer thicknesses of commonly used phosphatidylcholines as a function of temperature. *Biochim. Biophys. Acta.* 1808:2761–2771.
41. Sali, A., and T. L. Blundell. 1993. Comparative protein modelling by satisfaction of spatial restraints. *J. Mol. Biol.* 234:779–815.
42. Stansfeld, P. J., J. E. Goose, …, M. S. Sansom. 2015. MemProtMD: automated insertion of membrane protein structures into explicit lipid membranes. *Structure.* 23:1350–1361.
43. O'Connell, A. M., R. E. Koeppe, 2nd, and O. S. Andersen. 1990. Kinetics of gramicidin channel formation in lipid bilayers: transmembrane monomer association. *Science.* 250:1256–1259.
44. Lundbaek, J. A., S. A. Collingwood, …, O. S. Andersen. 2010. Lipid bilayer regulation of membrane protein function: gramicidin channels as molecular force probes. *J. R. Soc. Interface.* 7:373–395.
45. Lindblom, G., and L. Rilfors. 1989. Cubic phases and isotropic structures formed by membrane lipids — possible biological relevance. *Biochimica et Biophysica Acta (BBA) - Reviews on Biomembranes.* 988:221–256.
46. Shearman, G. C., A. I. I. Tyler, …, J. M. Seddon. 2010. Ordered micellar and inverse micellar lyotropic phases. *Liq. Cryst.* 37:679–694.
47. Phillips, R., T. Ursell, …, P. Sens. 2009. Emerging roles for lipids in shaping membrane-protein function. *Nature.* 459:379–385.
48. Bavi, O., M. Vossoughi, …, Y. Jamali. 2014. The effect of local bending on gating of MscL using a representative volume element and finite element simulation. *Channels (Austin).* 8:344–349.
49. Cantor, R. S. 1997. Lateral pressures in cell membranes: a mechanism for modulation of protein function. *J. Phys. Chem. B.* 101:1723–1725.
50. Baconguis, I., C. J. Bohlen, …, E. Gouaux. 2014. X-ray structure of acid-sensing ion channel 1-snake toxin complex reveals open state of a Na(+)-selective channel. *Cell.* 156:717–729.
51. Gonzales, E. B., T. Kawate, and E. Gouaux. 2009. Pore architecture and ion sites in acid-sensing ion channels and P2X receptors. *Nature.* 460:599–604.
52. Kellenberger, S., and T. Grutter. 2015. Architectural and functional similarities between trimeric ATP-gated P2X receptors and acid-sensing ion channels. *J. Mol. Biol.* 427:54–66.
53. Hattori, M., and E. Gouaux. 2012. Molecular mechanism of ATP binding and ion channel activation in P2X receptors. *Nature.* 485:207–212.
54. Canessa, C. M., L. Schild, …, B. C. Rossier. 1994. Amiloride-sensitive epithelial Na+ channel is made of three homologous subunits. *Nature.* 367:463–467.
55. Firsov, D., L. Schild, …, B. C. Rossier. 1996. Cell surface expression of the epithelial Na channel and a mutant causing Liddle syndrome: a quantitative approach. *Proc. Natl. Acad. Sci. USA.* 93:15370–15375.
56. Dawson, R. J., J. Benz, …, A. Ruf. 2012. Structure of the acid-sensing ion channel 1 in complex with the gating modifier Psalmotoxin 1. *Nat. Commun.* 3:936.
57. Gründer, S., and K. Augustinowski. 2012. Toxin binding reveals two open state structures for one acid-sensing ion channel. *Channels (Austin).* 6:409–413.
58. Wiggins, P., and R. Phillips. 2005. Membrane-protein interactions in mechanosensitive channels. *Biophys. J.* 88:880–902.
59. Ilyaskin, A. V., A. Diakov, …, S. Haerteis. 2017. Bile acids potentiate proton-activated currents in Xenopus laevis oocytes expressing human acid-sensing ion channel (ASIC1a). *Physiol. Rep.* 5:e13132.
60. Ilyaskin, A. V., A. Diakov, …, S. Haerteis. 2016. Activation of the human epithelial sodium channel (ENaC) by bile acids involves the degenerin site. *J. Biol. Chem.* 291:19835–19847.
61. Marra, S., R. Ferru-Clément, …, E. Deval. 2016. Non-acidic activation of pain-related acid-sensing ion channel 3 by lipids. *EMBO J.* 35:414–428.